

On the Determination of Age of Air Trends from Atmospheric Trace Species

ROLANDO R. GARCIA, WILLIAM J. RANDEL, AND DOUGLAS E. KINNISON

National Center for Atmospheric Research, Boulder, Colorado*

(Manuscript received 8 April 2010, in final form 19 August 2010)

ABSTRACT

Trace chemical species have been used in numerical models to calculate the age of air (AOA), which is a measure of the strength of the mean meridional circulation. The trend in the AOA has also been computed and found to be negative in simulations where greenhouse gases increase with time, which is consistent with the acceleration of the mean meridional circulation calculated under these conditions. This modeling result has been tested recently using observations of SF₆, a very long lived species whose atmospheric concentration has increased rapidly over the last half century, and of CO₂, which is also very long lived and increasing with time. Surprisingly, the AOA estimated from these gases exhibits no significant trend over the period 1975–2005. Here the Whole Atmosphere Community Climate Model (WACCM) is used to derive estimates of the AOA from SF₆ and CO₂ over the period 1965–2006. The calculated AOA yields trends that are smaller than the trend derived from a synthetic, linearly growing tracer, even after accounting for the nonlinear growth rates of SF₆ and CO₂. A simplified global transport model and analytical arguments are used to show that this follows from the variable growth rate of these species. It is also shown that, when AOA is sampled sparsely as in the observations, the resulting trends have very large error bars and are statistically undistinguishable from zero. These results suggest that trends in the AOA are difficult to estimate unambiguously except for well-sampled tracers that increase linearly and uniformly. While such tracers can be defined in numerical models, there are no naturally occurring species that exhibit such idealized behavior.

1. Introduction

The mean stratospheric age of air (AOA) may be defined as the interval between the time when the mixing ratio of a monotonically increasing tracer reaches a certain value χ at some location in the stratosphere and the (earlier) time when the same mixing ratio was reached at a reference location (usually in the tropical upper troposphere):

$$\Gamma = t(\chi; \theta, z) - t(\chi; \theta_0, z_0), \quad (1)$$

where (θ_0, z_0) are the latitude and altitude coordinates of the reference location and (θ, z) are the coordinates of any point in the meridional plane (cf. Hall and Plumb 1994; Waugh and Hall 2002).

AOA has several applications as a proxy for the stratospheric mean meridional circulation, or Brewer–Dobson (BD) circulation. Its absolute value has been used to assess whether the BD circulation computed in numerical models is too weak or too strong (e.g., Eyring et al. 2006), and its trend has been used to infer changes in the BD circulation. In particular, AOA trends are found to be negative (i.e., the AOA becomes younger) in simulations of the twentieth and twenty-first centuries carried out with climate–chemistry models that include observed and projected increases in greenhouse gases (GHGs), which is consistent with the trends in the BD circulation determined by direct examination of the mean meridional velocity field (Butchart et al. 2006; Austin et al. 2007; Li et al. 2008; Garcia and Randel 2008; McLandress and Shepherd 2009).

The tracer used in models to determine the AOA and its trend is usually a synthetic species with no sinks and a spatially uniform, linearly increasing source at ground level. However, very long lived natural tracers such as sulfur hexafluoride (SF₆) or carbon dioxide (CO₂) should be suitable for the same purpose since their abundance increases monotonically with time and they do not have any sinks below the upper mesosphere. In fact, an estimate

* The National Center for Atmospheric Research is sponsored by the National Science Foundation.

Corresponding author address: Rolando R. Garcia, National Center for Atmospheric Research, Boulder, CO 80307–1000.
E-mail: rgarcia@ucar.edu

of the trend in the AOA has been obtained recently by Engel et al. (2009) using a combination of SF₆ and CO₂ observations made between 32° and 41°N in the middle stratosphere from 1975 through 2005. Surprisingly, this determination did not yield a negative trend in the AOA; instead, Engel et al. reported a mean trend of 0.24 ± 0.22 yr decade⁻¹, which fails to support the model-derived results cited above. It should be noted that this does not contradict all model results since uncertainty in the trend estimate is large enough to overlap the trend estimates obtained from at least some models. Thus, the quoted standard deviation, $\sigma = 0.22$ yr decade⁻¹, implies that the observed AOA trend lies between 0.68 and -0.20 yr decade⁻¹ at the 95% (2σ) level. By comparison, the AOA trend obtained from recent simulations using a synthetic, linearly increasing tracer in the Whole Atmosphere Community Climate Model (WACCM, see below) is about -0.15 yr decade⁻¹, which falls within the 95% probability range of the AOA trend determined from the observations.

Here we investigate the problem of determining AOA trends from natural tracers by first obtaining AOA trends over the period 1965–2006 from WACCM simulations. The trends determined from zonal-mean, monthly-mean output for SF₆ and CO₂, although negative, are weak and subject to large uncertainties when the model output is sampled sparsely, as in observations. We interpret these results by means of a simple global model for conserved tracers, together with analytical arguments. The configuration of WACCM and the determination of AOA from modeled SF₆, CO₂, and a synthetic, linearly increasing tracer are discussed in sections 2 and 3. In section 4 we introduce a simple global model and show that it is capable of reproducing remarkably well the AOA results obtained with WACCM. In section 5 we construct simplified analytical solutions for the AOA and its trend and use these results to explain why model AOA trends computed from species such as SF₆ and CO₂ are ambiguous proxies for trends in the BD circulation (even though the mean values of AOA are in reasonably good agreement for SF₆, CO₂, and the synthetic linear tracer). The last section discusses the implications of these results for the experimental determination of AOA trends.

2. The Whole Atmosphere Community Climate Model

WACCM is a global climate model with fully coupled chemistry, radiation, and dynamics; a full description has been given recently by Garcia et al. (2007). The present version of WACCM differs from that model in several respects, to wit: The chemistry module has been updated according to the JPL-2006 recommendations (Sander et al.

2006); a quasi-biennial oscillation (QBO) is imposed by relaxing the winds to observations in the tropics (Matthes et al. 2004); heating from volcanic aerosols is now computed (Tilmes et al. 2009); the effect of unresolved orography is parameterized as surface stress (Holstlag and Boville 1993; Richter et al. 2010); and gravity waves due to convective and frontal sources are parameterized based on the occurrence of convection and the diagnosis of regions of frontogenesis in the model (Richter et al. 2010). For gravity waves forced by orography, the parameterization of McFarlane (1987) is retained unchanged from the previous version.

For the present study we used WACCM to simulate the evolution of SF₆, CO₂, and a synthetic tracer over the period 1953–2006. The synthetic tracer, hereafter referred to as AOA1, has no sinks and is specified to have a uniform mixing ratio at the lower boundary that increases linearly with time. Boundary conditions for GHGs and other chemical species are identical to those used in simulations defined by the second Chemistry–Climate Model Validation Project (CCMVal-2) of the Stratospheric Processes and their Role in Climate (SPARC) project, as described by Eyring et al. (2008). In addition, sea surface temperatures were taken from the Hadley–Reynolds dataset (Hurrell et al. 2006) and a QBO was imposed by relaxing tropical stratospheric winds to the data compiled by Giorgetta for CCMVal-2 (Eyring et al. 2008). Two independent realizations of these simulations were carried out.

SF₆ is not commonly calculated in chemistry–climate models because it has no impact on either the chemistry of other trace species or on the radiative budget of the atmosphere. Thus, SF₆ is not part of the boundary conditions specified by CCMVal-2. For the present simulations, we define a source at ground level that varies with latitude and time according to observations (Maiss and Brenninkmeijer 1998), extended as recommended by the Carbon Dioxide Information Analysis Center (CDIAC) of the U.S. Department of Energy (http://cdiac.ornl.gov/oceans/new_atmCFC.html). Loss of SF₆ occurs only through photolysis at Lyman-alpha wavelengths, for which we have used the absorption coefficients from Pradayrol et al. (1996).

3. Determination of age of air from trace species simulated with WACCM

Age of air is determined from Eq. (1) using monthly and zonally averaged output for each trace species of interest. The reference point was chosen as

$$(\theta_0, z_0) = (0.9^\circ, 149 \text{ mb}), \quad (2)$$

which is the WACCM grid point closest to the equator in the upper troposphere. The choice of a base point is somewhat arbitrary since AOA results are not sensitive

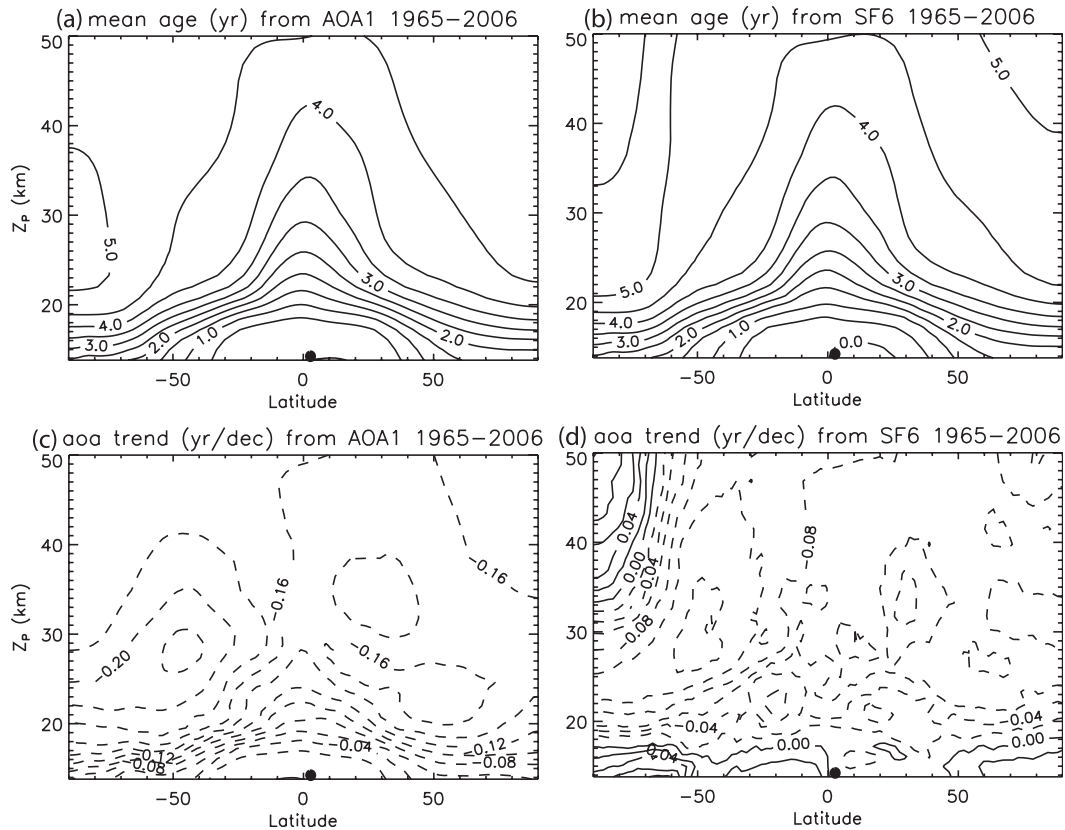


FIG. 1. Stratospheric mean age of air and its trend in the meridional plane estimated from WACCM simulations of (a),(c) the linearly increasing, synthetic tracer AOA1 and (b),(d) SF₆. The black dots denote the location of the base point used to calculate age of air; SF₆ ages were corrected for nonlinear growth as discussed in the text.

to its location as long as it lies within the tropical upper troposphere. Figure 1 shows the AOA and its trend in the latitude–altitude plane derived from the synthetic tracer, AOA1, and from SF₆ for one of the WACCM simulations (the second simulation yields statistically identical results). The trends are determined via a linear fit to the model output versus time beginning in 1965; the first 12 yr of the simulation (1953–64) are discarded because the AOA1 is initialized to have zero abundance, and SF₆ itself has nearly zero abundance in 1953, so the distributions of these tracers must be allowed to reach quasi-steady-state equilibria throughout the stratosphere before the AOA can be accurately estimated from them. When calculating the AOA from SF₆, a correction has been applied to account for the nonlinear growth of this species, per Eq. (12) of Hall and Plumb (1994), using $\Delta^2/\Gamma = 0.8$, where Δ is the width of the age spectrum and Γ is the mean age. Hall and Plumb showed that Δ^2/Γ is relatively constant throughout the stratosphere; the value 0.8 is on the upper part of the range of stratospheric values estimated by Hall and Plumb (see their Fig. 9). Smaller values would give smaller corrections to the AOA, but with the value used here the mean AOA distributions for

the linear tracer, AOA1, and SF₆ shown in Fig. 1 are in good agreement throughout most of the stratosphere. Nevertheless, the AOA trend computed from SF₆ is roughly half of that obtained from AOA1 at most locations in the stratosphere.

Figure 2 shows the evolution of the AOA computed from SF₆, and its linear trend, at two locations: in the midlatitude stratosphere of the Northern Hemisphere (40.7°N, 20.1 mb) and in the tropical middle stratosphere (0.9°N, 10.7 mb). The first is chosen to facilitate comparison with the results of Engel et al. (2009), which are derived from data taken above 30 mb over the range of latitude 32°–51°N. The second location is more appropriate for comparison with earlier estimates from WACCM reported by Garcia et al. (2007) and with the results of the global transport model presented in section 4. In northern midlatitudes (Figs. 2a,b), the trend computed from AOA1 is significant and negative, amounting to -0.154 ± 0.007 yr decade⁻¹, but the trend computed from SF₆, while also significant, is much weaker: -0.086 ± 0.011 yr decade⁻¹. Similar results are obtained in the tropical stratosphere for the AOA trend (Figs. 2c,d), which is -0.146 ± 0.009 yr decade⁻¹ for AOA1 but

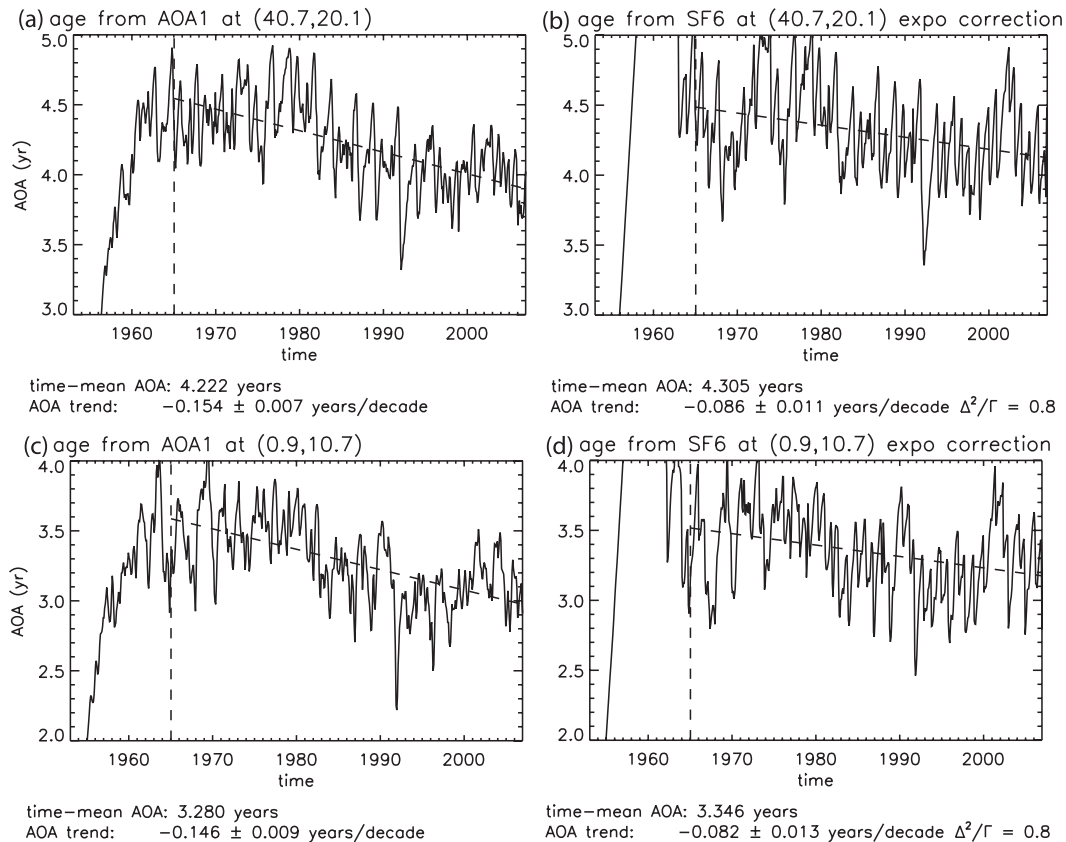


FIG. 2. Stratospheric mean age of air and its trend estimated from WACCM simulations of the linearly increasing, synthetic tracer AOA1 and of SF₆. Mean ages and trends at (a),(b) 40.7°N, 20.1 mb and (c),(d) 0.9°N, 10.7 mb. The period 1953–64, inclusive, which is affected by the initial conditions, is not used in the linear trend determination. The linear trend is indicated by the dashed line in each panel; SF₆ ages are corrected for nonlinear growth.

-0.082 ± 0.013 yr decade⁻¹ for SF₆. The age of air itself is younger in the tropics than in midlatitudes, as expected. The standard deviation of the modeled AOA trend is much smaller than that of the trend derived from observations by Engel et al. (2009), which is not surprising since the former is averaged in space (zonal means) and time (monthly means), whereas the latter consist of local observations with sparse sampling in time.¹ The WACCM results also differ from Engel et al.'s estimates in that the mean value of the AOA is somewhat younger in the model (4.2 yr for AOA1 and 4.3 yr for SF₆ in midlatitudes, averaged over the period 1965–2007) than deduced from the observations (about 4.9 yr).

The foregoing raises the question whether trends in AOA determined from other modeled tracers are in better agreement with the trend calculated from the synthetic tracer AOA1. In particular, CO₂, with its very

long lifetime, should be suitable for determining AOA and its trend; Engel et al. (2009) used the AOA derived from this gas, as well as from SF₆, to infer that AOA has not become younger in the period 1975–2005. Figure 3 shows that the AOA trends from CO₂ are about -0.06 and -0.1 yr decade⁻¹ in the midlatitude and tropical stratosphere, respectively. These values are again substantially smaller than the trends calculated from AOA1 (cf. Fig. 2c). Further, the AOA time series obtained from CO₂ exhibit very large interannual variability, as much as ± 1 yr, which arises from the large seasonal cycle of CO₂ at the reference point (2) used to calculate AOA. In a model with continuous output, the problem can be addressed by smoothing the CO₂ time series at the reference point with a 13-month running mean before computing the AOA. However, the resulting AOA trends, shown in the right column of Fig. 3, are still much smaller than the trends computed from AOA1.

In summary, although WACCM calculations of the natural tracers SF₆ and CO₂ yield negative trends in AOA, these trends are substantially weaker than the trend

¹ If the model output is sampled sparsely, as in the observations, the estimated AOA trends become much more uncertain, and can even be positive. We address this point in section 6.

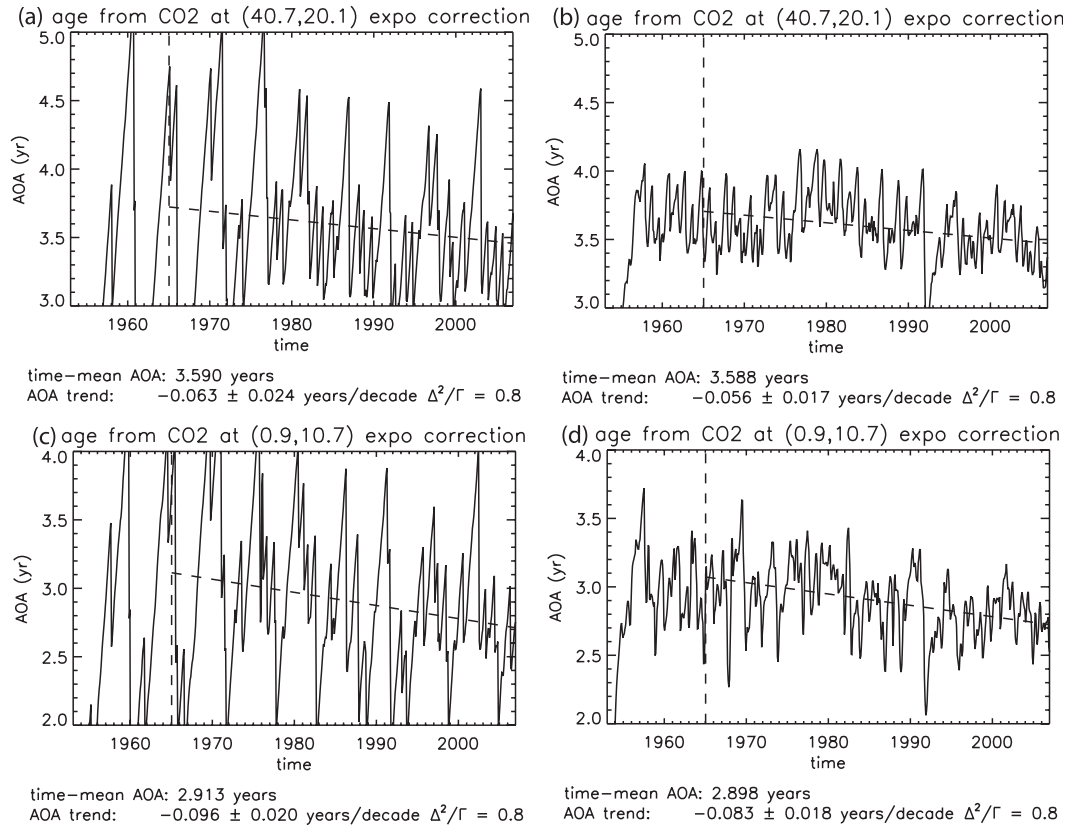


FIG. 3. Stratospheric mean age of air and its trend determined from WACCM CO₂ in (a),(b) the midlatitude stratosphere (40.7°N, 20.1 mb) and (c),(d) the tropical stratosphere (0.9°N, 10.7 mb). In the results shown in the right column, CO₂ at the entry point into the stratosphere was smoothed with a 13-month running mean to remove the annual cycle before computing AOA and its trend. The linear trend is indicated by the dashed line in each panel. CO₂ ages are corrected for nonlinear growth.

derived from the synthetic linear tracer, AOA1. In the model, the transformed Eulerian mean (TEM) vertical velocity \bar{w}^* strengthens at the rate of about 2%–2.5% decade⁻¹ in the tropical lower stratosphere, averaged over $\pm 22^\circ$ and 100–10 mb (not shown). This is about one-half the percentage change in AOA derived from AOA1, which is -0.15 yr decade⁻¹, or 4.5% decade⁻¹ referred to the mean age of 3.3 yr determined from AOA1 in the tropics (Fig. 2). We show below, in section 4, that this factor of 2 difference between the percentage change in AOA and the percentage change in \bar{w}^* is predicted by a simple global model of the stratospheric circulation. We shall also use this model to interpret why AOA trends derived from SF₆ and CO₂ do not match that obtained from AOA1.

4. A one-dimensional global model for conservative trace species

a. Governing equations

Holton (1986) showed that the global profiles of a chemical trace species can be described by means of a

simple model wherein the tracer distribution is represented by a global mean $\hat{\chi}$ plus zonally averaged and zonally asymmetric deviations therefrom, $\bar{\chi}$ and χ' :

$$\chi(\theta, z, t) = \hat{\chi}(z, t) + \bar{\chi}(\theta, z, t) + \chi'(\lambda, \theta, z), \quad (3)$$

where λ , θ , z , and t are longitude, latitude, log-pressure altitude, and time, respectively. This allows for changes in the zonal mean and global mean mixing ratio but assumes that eddy amplitudes remain constant. Substitution of Eq. (3) into the TEM chemical continuity equation in log-pressure coordinates leads to an equation for the global-mean mixing ratio:

$$\frac{\partial \hat{\chi}}{\partial t} + \left\langle \frac{1}{\rho} \frac{\partial}{\partial z} (\rho \bar{w}^* \bar{\chi}) \right\rangle = 0, \quad (4)$$

where the angle brackets denote the global average, and to an equation that describes the balance between vertical advection and horizontal eddy transport:

TABLE 1. Time variability of the vertical velocity in the simple global model.

Type	Specification	Comments
Trend	$W_2 = W_0(1 + st)$, Eq. (12)	W_0, s defined in Eq. (13)
Annual	$W_2\{1 + 0.25 \sin[2\pi(t - 0.25)]\}$	Maximum in NH spring
Quasi-biennial	$W_2\left\{1 + 0.5 \sin\left[mz + \frac{2\pi t}{2.33 \text{ yr}}\right]\right\}$	$m = 2\pi/30 \text{ km}^{-1}$
Volcanic	$W_2\left\{1 + 0.75 \exp\left[-\frac{1}{2}\left(\frac{z - 10 \text{ km}}{5 \text{ km}}\right)^2\right] \exp\left[-\left(\frac{t - t_0}{0.33 \text{ yr}}\right)\right]\right\}$	$t_0 = 1963, 1982, 1991$

$$\bar{w}^* \frac{\partial \hat{\chi}}{\partial z} = \frac{K_{yy}}{a^2} \frac{\partial}{\partial \mu} \left[(1 - \mu^2) \frac{\partial \hat{\chi}}{\partial \mu} \right], \quad (5)$$

where the eddy flux has been expressed as eddy diffusion with a constant diffusion coefficient K_{yy} , $\mu = \sin\theta$, θ is latitude, a is the earth's radius, z is log-pressure altitude, and ρ is the density in the log-pressure system [see Holton (1986) for details].

A solution to Eqs. (4) and (5) is obtained by expressing the latitudinal dependence of \bar{w}^* and $\bar{\chi}$ in terms of the Legendre polynomial of second degree, $P_2 = 0.5(3\mu^2 - 1)$, as follows:

$$[\bar{\chi}(\mu, z, t), \bar{w}^*(\mu, z, t)] = [X_2(z, t), W_2(z, t)]P_2(\mu), \quad (6)$$

which leads to

$$\frac{\partial \hat{\chi}}{\partial t} + \frac{1}{\rho} \frac{\partial}{\partial z} \left(\frac{\rho W_2 X_2}{5} \right) = 0 \quad (7)$$

and

$$W_2 \frac{\partial \hat{\chi}}{\partial z} = -\frac{K_{yy}}{6a^2} X_2, \quad (8)$$

as explained by Holton (1986). Equations (7) and (8) can be combined to give a single one-dimensional (1D) advection–diffusion equation for the global mean mixing ratio:

$$\frac{\partial \hat{\chi}}{\partial t} + w_e \frac{\partial \hat{\chi}}{\partial z} - K_e \frac{\partial^2 \hat{\chi}}{\partial z^2} = 0, \quad (9)$$

where

$$K_e = \frac{a^2 W_2^2}{30 K_{yy}}; \quad w_e = \frac{K_e}{H} \quad (10)$$

are an effective vertical diffusion coefficient and an effective vertical velocity, respectively.

b. Numerical solutions

Equation (9) is solved in a domain $z \in (15, 50)$ km that encompasses the stratosphere, with a specified lower

boundary condition $\hat{\chi}(z_0, t)$. Below we present numerical solutions wherein the lower boundary condition, $\hat{\chi}(z_0, t)$, is set to the value of AOA1, SF₆, or CO₂ taken from WACCM output at the reference point (2) in the upper tropical troposphere. To complete the specification of the problem, we need to define the diffusion coefficient K_{yy} and the vertical and time dependence of the TEM vertical velocity field W_2 in Eq. (10). For the diffusion coefficient we take

$$K_{yy} = 2 \times 10^5 \text{ m}^2 \text{ s}^{-1}, \quad (11)$$

which may be considered a time-mean value encompassing seasons when its magnitude is estimated to be several times larger, as in northern winter, and other times when its value is essentially zero (see, e.g., Garcia 1991). To simulate a strengthening BD circulation we let

$$W_2 = -W_0(1 + st), \quad (12)$$

where

$$W_0 = 0.4 \times 10^{-3} \text{ m s}^{-1}; \quad s = 0.003 \text{ yr}^{-1}. \quad (13)$$

The negative sign in Eq. (12) is required to produce upwelling in the tropics and downwelling in extratropical latitudes because $\bar{w}^* = W_2 P_2$, per Eq. (6), and the latitude dependence of P_2 has the opposite sign. The value chosen for W_0 is representative of the vertical velocity computed with WACCM in the lower stratosphere, while the linear growth rate—3% decade⁻¹—is consistent with the acceleration of the BD circulation quoted in section 3.

Additional sources of variability in W_2 may be specified, as outlined in Table 1. These modify the definition (12) by including annual and quasi-biennial cycles, or even stochastic variability due to singular events such as volcanic eruptions, which enhance upwelling in the lower stratosphere through heating of volcanic aerosols. In the latter case, perturbations to the vertical velocity are introduced in the appropriate months of 1963, 1982, and 1991, which are years of major volcanic eruptions in the tropics. While these additional sources of variability turn out to be unimportant for the long-term evolution of the trace species (and, therefore, for the trend in the

AOA), it is instructive to include them because they explain some of the interannual variability seen in the AOA series simulated with WACCM.

Simulations of AOA derived from the AOA1, SF₆, and CO₂ time series obtained from numerical solution of Eq. (9) are shown in Fig. 4. In these solutions all of the sources of variability of the vertical velocity listed in Table 1 are included and the AOA is shown at the equator and 30-km log-pressure altitude (~10 mb) so that it can be compared directly with the WACCM results of Figs. 2 and 3. These AOA estimates are corrected per Eq. (35) of section 5, which is equivalent to Eq. (23) of Hall and Plumb (1994) and is appropriate for exponentially growing tracers in the 1D global model.

The time series of AOA obtained from the simple model bear a striking resemblance to those from WACCM, as do the AOA trends derived from them. For example, the influence of volcanic heating (which accelerates the circulation and decreases AOA) on the evolution of AOA derived from AOA1 and SF₆ can be seen clearly in Figs. 2c,d and 4a,b, especially after the eruptions of Agung (1963) and Mt. Pinatubo (1991). On the other hand, this influence is not apparent in the time series of AOA from CO₂ (Fig. 4c), which instead is dominated by the same very large interannual variability seen in Fig. 3 and discussed in section 2. All three time series also contain considerable quasi-biennial variability, which can be appreciated best in AOA1. Quasi-biennial variability is also present in the time series for SF₆ and CO₂, but it is less apparent there because these species exhibit additional variability that originates from the seasonal cycle in the lower boundary condition. Note that, although SF₆ does not have a seasonal cycle at ground level, it is produced mainly in the Northern Hemisphere, and this causes larger mixing ratios to occur in the tropical upper troposphere in boreal summer. The AOA trend derived from AOA1 in these calculations is strongly negative, while the trends from SF₆ and CO₂ are weaker, consistent with the results obtained from WACCM (Figs. 2 and 3). Furthermore, the actual values of the AOA trends are very similar in WACCM results and in the simple model: -0.149 versus -0.146 yr decade⁻¹ for AOA1 in the tropical stratosphere, -0.091 versus -0.086 yr decade⁻¹ for SF₆, and -0.087 versus -0.091 for CO₂.

Figure 5 shows time series of the AOA derived from AOA1 and SF₆ in the 1D global model, this time excluding all variability in the vertical velocity other than the long-term trend. Compared to Fig. 4, these time series exhibit less interannual variation, especially in the case of AOA1. AOA from SF₆ is more similar to its counterpart in Fig. 4 because, as noted above, a substantial amount of the variability in this species, and its AOA, originates from the lower boundary condition. However, it is clear

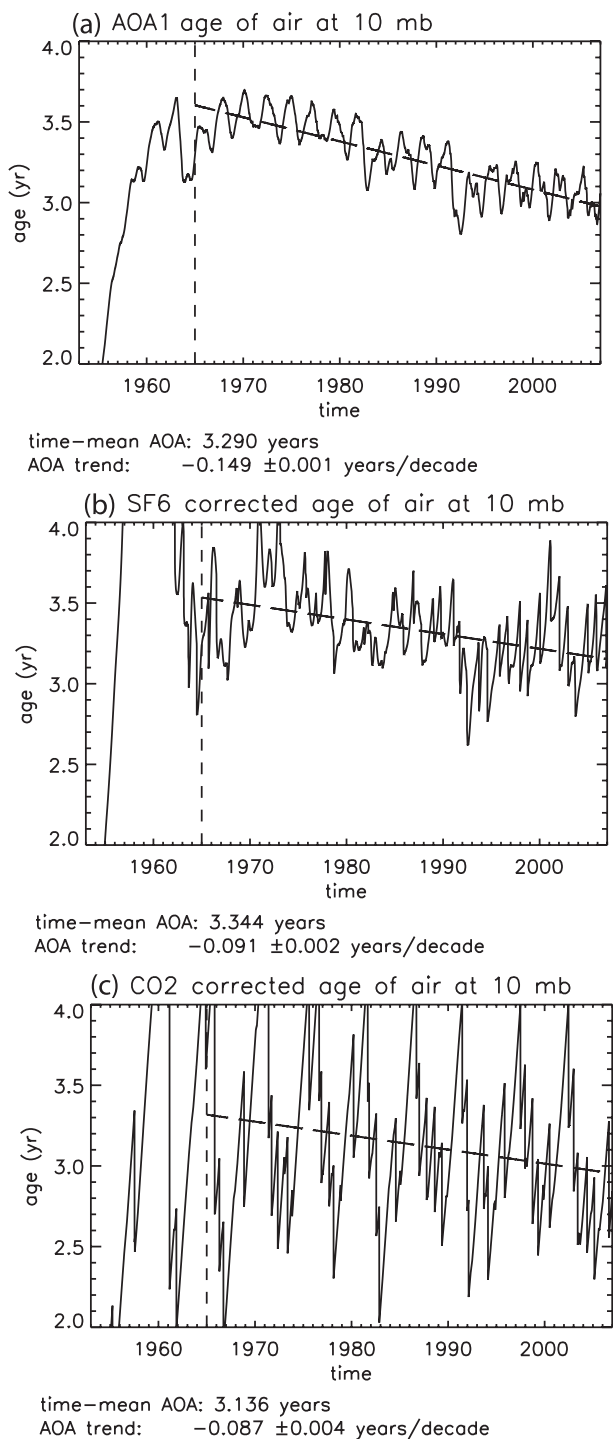


FIG. 4. Stratospheric mean age of air and its trend at 10 mb estimated from the simple model of section 4 for (a) the synthetic tracer AOA1, (b) SF₆, and (c) CO₂. The linear trend is indicated by the dashed line in each panel; SF₆ and CO₂ ages were corrected for nonlinear growth as discussed in the text.

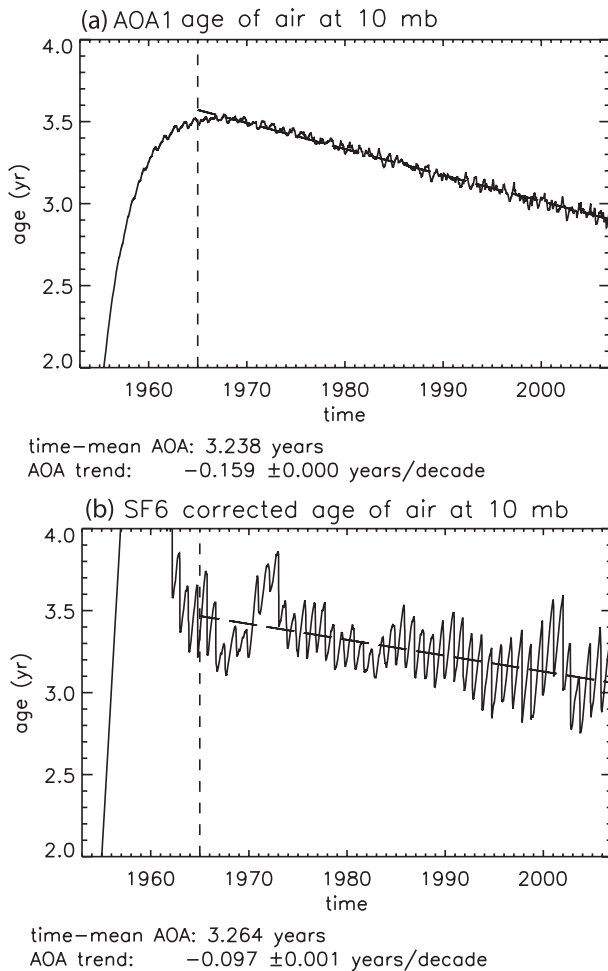


FIG. 5. As in Fig. 4, but excluding all sources of variability in the vertical velocity except the secular trend.

from comparison of Figs. 4 and 5 that, while the addition of variability to the vertical velocity field produces series of AOA that resemble more closely those obtained from WACCM, such variability does not alter much the long-term trend in AOA. Trend values for the AOA derived from AOA1 are strongly negative and very similar in Figs. 4 and 5, whereas trends in the AOA derived from SF₆ are weaker. Note, however, that the velocity perturbation due to the eruption of Mt. Agung in 1963 introduces a positive bias in the trends shown in Fig. 4 because it lowers substantially the AOA for a couple of years following the eruption. This is why the AOA trends of Fig. 4 are less negative than the respective trends in Fig. 5. Similar results (not shown) are obtained for CO₂.

These results suggest that the principal features of the AOA time series can be simulated accurately with our simple model. But, why does AOA computed from SF₆ or from CO₂ behave differently from AOA computed from the linear tracer AOA1? In the next section we

attempt to elucidate this question by obtaining analytical solutions to the 1D global model.

5. Analytical solutions for age of air

We provide approximate solutions to Eq. (9) for two special cases relevant to understanding the behavior of AOA derived from trace species with different growth rates: a linearly growing species, like AOA1, and a species with a fast exponential growth rate (which mimics the behavior of SF₆). The heuristic approach used here yields solutions for AOA consistent with those obtained previously by Hall and Plumb (1994) using the Green's function of Eq. (9). Although these solutions lack the generality of the Green's function method, their relative simplicity allows us to make inferences about the behavior of trends in AOA, a topic that was not addressed by Hall and Plumb.

a. Linearly growing tracer

For a linearly increasing tracer, the lower boundary condition may be written as

$$\hat{\chi}(z_0, t) = X_0 + r_1 t, \quad (14)$$

where r_1 is the growth rate, in units of mixing ratio per time. We then assume the system is near enough to equilibrium that the mixing ratio everywhere in the domain also grows as $r_1 t$, in which case Eq. (9) may be rewritten as

$$\frac{\partial^2 \hat{\chi}}{\partial z^2} - \frac{w_e}{K_e} \frac{\partial \hat{\chi}}{\partial z} - \frac{r_1}{K_e} = 0 \quad (15)$$

or

$$\frac{\partial}{\partial z} \left[\frac{\partial \hat{\chi}}{\partial z} \exp\left(-\frac{w_e z}{K_e}\right) \right] = \frac{r_1}{K_e} \exp\left(-\frac{w_e z}{K_e}\right). \quad (16)$$

Assuming that w_e is not a function of z , this has the solution

$$\hat{\chi}(z, t) = \hat{\chi}(z_0, t) - \frac{r_1 z}{w_e} + H \left[\left(\frac{\partial \hat{\chi}}{\partial z} \right)_{z_0, t} + \frac{r_1}{w_e} \right] (e^{z/H} - 1), \quad (17)$$

where we have used the relationship $w_e = K_e/H$ from Eq. (10). The term in brackets on the rhs of Eq. (17) must vanish after the vertical profile of $\hat{\chi}$ has equilibrated since, in that case,

$$\frac{\partial \hat{\chi}(z, t)}{\partial t} \rightarrow r_1 \quad \forall z \quad (18)$$

by assumption, which cannot be satisfied unless the term in question is zero. Then, the equilibrium profile of the linearly growing tracer is just

$$\hat{\chi}(z, t) = \hat{\chi}(z_0, t) - \frac{r_1 z}{w_e}, \quad (19)$$

such that $\hat{\chi}$ decreases linearly with altitude above the lower boundary. To obtain the AOA from Eq. (17), we set $\hat{\chi}(z, t) = \hat{\chi}(z_0, t - \Gamma)$ whence, with the aid of Eq. (14), it follows that

$$\Gamma = \frac{z}{w_e} - \frac{H}{r_1} \left[\left(\frac{\partial \hat{\chi}}{\partial z} \right)_{z_0, t} + \frac{r_1}{w_e} \right] (e^{z/H} - 1). \quad (20)$$

Under the same assumptions that led to Eq. (19) this reduces to

$$\Gamma = \frac{z}{w_e}, \quad (21)$$

which states that the AOA for the linearly growing tracer is the ‘‘advective time scale’’ z/w_e . Equations (19) and (21) for the equilibrium profile and AOA, respectively, coincide with the results obtained by Hall and Plumb (1994) from the Green’s function solution to the same advection–diffusion model used here. However, these equations do not predict how AOA evolves when the vertical profile of the tracer is not in equilibrium, such that the terms in brackets in Eqs. (17) and (20) are not zero. We shall see below that consideration of this effect is important for understanding the evolution of AOA.

A trend in AOA for the linear tracer can be obtained from Eq. (21) if we specify a trend in the circulation as given by Eq. (12)—that is, $W_2 \sim (1 + st)$. Then, using the relationship (10) between w_e and W_2 , we have

$$\Gamma = \frac{z}{w_{e0}} \frac{1}{(1 + st)^2}, \quad (22)$$

where $w_{e0} = w_e(t = 0)$ and the quadratic nature of the time-dependent term comes from the fact that $w_e \sim (W_2)^2$, per Eq. (10). Finally, taking into account that the rate of change s is small, such that $st \gg 1$ even over a 50-yr period, we obtain for the trend in AOA

$$\frac{d\Gamma}{dt} = -2s \frac{z}{w_{e0}}. \quad (23)$$

For an accelerating circulation, such as we have assumed here, this trend is always negative and independent of the growth rate of the tracer, in agreement with the results for AOA1 shown in Figs. 4 and 5. Note that, within the scope of

the approximations made in their derivation, we can infer from Eqs. (21) and (23) that the fractional, or percentage, AOA change in a linearly growing tracer, $\delta\Gamma/\Gamma$, should be twice as large as the corresponding change in the circulation, $\delta w^*/w^*$ (and, of course, of the opposite sign). This is consistent with the result quoted at the end of section 2 that, in WACCM, the magnitude of the AOA trend obtained from the linear tracer, AOA1, is roughly twice as large as the trend in the BD circulation.

b. Exponentially growing tracer

For an exponentially increasing tracer we assume a lower boundary condition

$$\hat{\chi}(z_0, t) = X_0 \exp(r_2 t), \quad (24)$$

where r_2 is the growth rate, in units of inverse time. We then proceed as in the case of linear growth so that Eq. (9) becomes

$$\frac{\partial^2 \hat{\chi}}{\partial z^2} - \frac{w_e}{K_e} \frac{\partial \hat{\chi}}{\partial z} - \frac{r_2}{K_e} \hat{\chi} = 0, \quad (25)$$

which has the solution

$$\hat{\chi}(z, t) = A_1 \exp(m_1 z) + A_2 \exp(m_2 z), \quad (26)$$

where

$$(m_1, m_2) = \frac{1}{2H} \left(1 \pm \sqrt{1 + \frac{4r_2 H}{w_e}} \right) \quad (27)$$

and the constants A_1 and A_2 are evaluated in terms of the boundary conditions at $z = z_0$:

$$\hat{\chi}(z_0, t) = A_1 + A_2; \quad \left(\frac{\partial \hat{\chi}}{\partial z} \right)_{z_0, t} = m_1 A_1 + m_2 A_2. \quad (28)$$

Substitution into Eq. (26) leads to

$$\hat{\chi}(z, t) = \hat{\chi}(z_0, t) \exp(m_2 z) \left\{ 1 + H' \left[\left(\frac{1}{\hat{\chi}} \frac{\partial \hat{\chi}}{\partial z} \right)_{z_0, t} - m_2 \right] \times (e^{z/H'} - 1) \right\}, \quad (29)$$

where

$$\frac{1}{H'} = \frac{1}{H} \sqrt{1 + \frac{4r_2 H}{w_e}} \quad (30)$$

and m_2 is given by Eq. (27). As in the linear growth case, once the profile equilibrates, the term inside the square

brackets in Eq. (29) must vanish, such that the equilibrium profile becomes

$$\hat{\chi}(z, t) = \hat{\chi}(z_0, t) \exp(m_2 z). \quad (31)$$

Therefore, the equilibrium profile for an exponentially growing tracer is itself exponential. We obtain the AOA from Eq. (29) as in the case of the linear profile, which yields

$$\Gamma_e = -\frac{m_2 z}{r_2} - \frac{1}{r_2} \ln \left\{ 1 + H' \left[\left(\frac{1}{\hat{\chi}} \frac{\partial \hat{\chi}}{\partial z} \right)_{z_0, t} - m_2 \right] (e^{z/H'} - 1) \right\}, \quad (32)$$

with m_2 given by Eq. (27). Once the profile has equilibrated, this reduces to

$$\Gamma_e = \frac{z}{2r_2 H} \left(\sqrt{1 + \frac{4r_2 H}{w_e}} - 1 \right). \quad (33)$$

This can be rewritten as

$$\Gamma_e = \Gamma \left(\frac{w_e}{2r_2 H} \right) \left(\sqrt{1 + \frac{4r_2 H}{w_e}} - 1 \right), \quad (34)$$

where Γ is the ‘‘advective’’ AOA given by Eq. (21). Equation (34) is equivalent to Eq. (23) of Hall and Plumb (1994). Using this expression, the advective AOA can be obtained from the AOA for an exponentially growing tracer as

$$\Gamma = \Gamma_e \left[\left(\frac{w_e}{2r_2 H} \right) \left(\sqrt{1 + \frac{4r_2 H}{w_e}} - 1 \right) \right]^{-1}. \quad (35)$$

For small $r_2 H/w_e$, the square root term in Eq. (34) can be expanded to second order in that quantity to yield

$$\Gamma_e = \Gamma \left(1 - \frac{r_2 H}{w_e} \right), \quad (36)$$

which is the counterpart of Eq. (12) of Hall and Plumb (1994) in the 1D global model and states that Γ_e depends on the growth rate of the tracer r_2 and becomes smaller as r_2 increases and longer as it decreases, approaching the result for the linear tracer Γ as $r_2 \rightarrow 0$.

c. Comparison with the numerical solutions

How well do the analytical solutions describe the behavior of AOA in the 1D global model? Figure 6 shows AOA time series obtained from numerical solution of

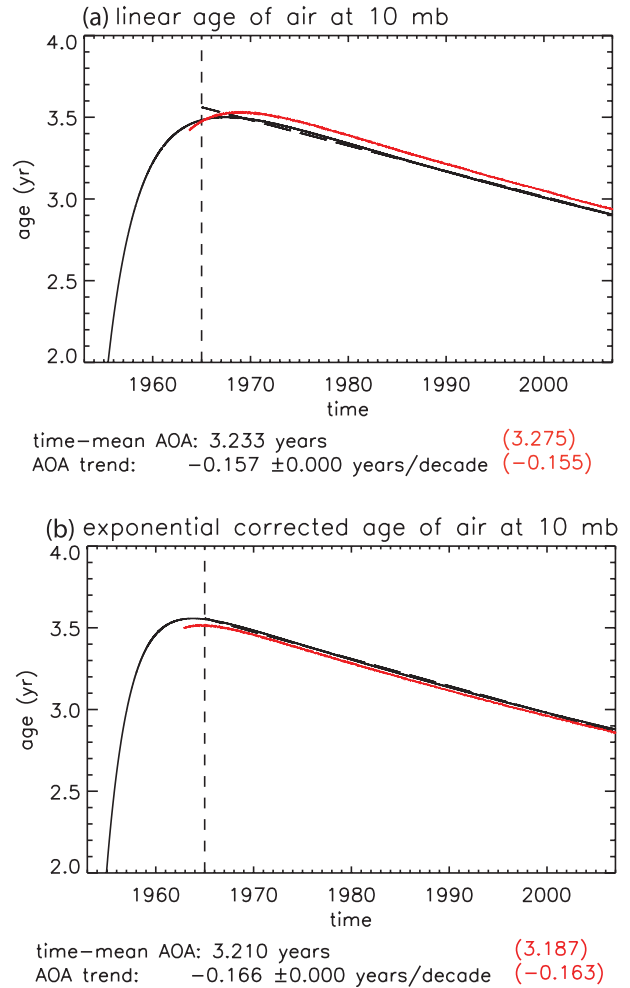


FIG. 6. Numerical (black) and analytical (red) solutions for AOA derived from (a) a linearly growing tracer and (b) an exponentially growing tracer. The dashed black lines are linear fits to the numerical solutions excluding the period affected by the initial conditions. The AOA and its trend for the analytical solution are shown in red, in parentheses. The AOA of the exponential tracer is corrected for nonlinear growth.

Eq. (9) for two idealized specifications of the lower boundary condition, $\hat{\chi}(z_0, t)$. In the first case (Fig. 6a), $\hat{\chi}$ is defined to have a linear growth rate, as in Eq. (14), while in the second case (Fig. 6b) it is defined to grow exponentially, per Eq. (24). The growth rate for the linear case was set to the same value as the rate of increase of the AOA1 tracer in the WACCM simulations (although this detail is unimportant since, as seen in section 5a, the AOA in the linear case is independent of the growth rate). In the exponential case, the growth rate was taken to be $r_2 = 0.15 \text{ yr}^{-1}$, which is typical of the fast exponential growth rate of SF_6 in WACCM in the 1960s and 1970s. Superimposed on these solutions are the analytical solutions (20) and (32) derived above. In all examples

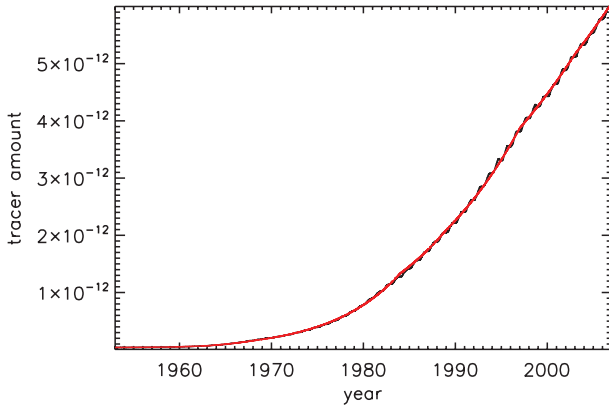


FIG. 7. Actual (black) and analytical (red) time series of SF₆ at the reference point used for calculations of AOA. See text for details.

shown, the vertical velocity has a secular trend, per Eq. (12), but no other sources of variability.

The agreement between numerical and analytical solutions is remarkably close, suggesting that the latter may be used to interpret the evolution of AOA. We note that the trend in AOA for the linear tracer is very similar to the trend obtained from AOA1, shown in Figs. 4a and 5a for various calculations with the 1D global model, and in Fig. 2c for the WACCM simulation. The AOA calculated for the exponentially growing tracer uses the correction (35). With this correction the AOA trend is $-0.16 \text{ yr decade}^{-1}$, consistent with that of the linear tracer, and of AOA1 in WACCM and larger than the trends derived from WACCM SF₆ and CO₂.

These results show that the behavior of the age of air derived from AOA1 is completely consistent with that expected for an idealized, linearly growing tracer. This is not surprising because AOA1 also grows linearly, aside from perturbations due to model interannual variability, which, however, do not contribute to the long-term trend. Thus, in the case of AOA1, we may consider the evolution of the age of air and its trend to be fully explained by the results for an equilibrated, linearly growing tracer, Eqs. (21) and (23). The same cannot be said for SF₆. The result shown in Fig. 6b indicates that the corrected AOA of an exponentially growing tracer should yield a trend close to that of AOA1 but, in fact, the trend derived from SF₆ in both WACCM and the 1D model is smaller. In the case of CO₂, the growth rate is slow enough that this species should behave like an idealized linear tracer but, again, AOA trends derived from WACCM CO₂ are smaller than those derived from AOA1.

To understand the factors that affect the evolution of the AOA derived from SF₆ and CO₂ we need to consider the details of the growth histories of these species over the period 1953–2006. Figure 7 shows the time series

TABLE 2. Specification of the time-dependent growth rate of the SF₆-like tracer.

Segment t_i (yr)	Growth rate (yr^{-1})
[1953, 1958]	0.025
[1959, 1962]	0.100
[1963, 1967]	0.165
[1968, 1983]	0.133
[1984, 1988]	0.090
[1989, 1996]	0.077
[1997, 2002]	0.048
[2003, 2006]	0.040

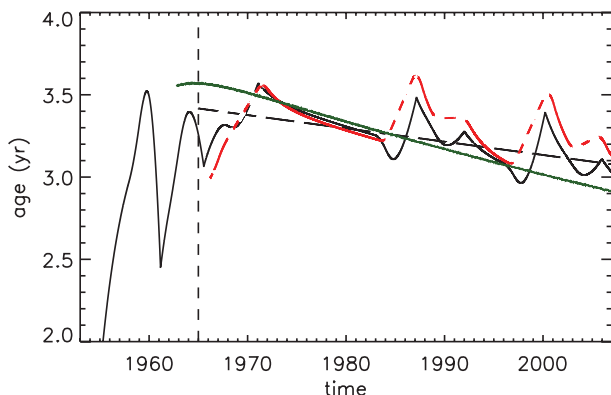
of SF₆ calculated with WACCM at the reference point (2), which is also used as the lower boundary condition in the 1D global model. Superimposed on the actual time series for SF₆ is the time series for an “SF₆-like” species, whose time dependence consists of several piecewise continuous segments:

$$\text{SF}_6(t_i) = \text{SF}_6(t_{0i}) \exp(r_i t_i), \quad (37)$$

where t_i denotes a period when the tracer grows at rate r_i , and t_{0i} is the initial time of each such period. These segments and their growth rates are shown in Table 2. It can be seen that the piecewise fit (37) captures faithfully the long-term evolution of SF₆.

We have calculated the AOA for the SF₆-like tracer using both the numerical and the analytical solution described in section 5, including no variability in the global-mean vertical velocity other than the long-term trend. The results are presented in Fig. 8, where the numerical solution is shown in black and the analytical solution in red.² In both cases, the AOA has been corrected for exponential growth according to Eq. (35). While the agreement between the two solutions is not as good as in the idealized cases shown in Fig. 6, the analytical solution still captures all the main features of the long-term evolution of AOA for the SF₆-like tracer. In particular, it is clear that the evolution of AOA is interrupted each time that there is a change in the growth rate of the tracer and that the result is a reduction of the long-term trend since the AOA seldom follows the time dependence expected from an exponentially growing tracer with a constant growth rate. The last point is highlighted by the green curve in Fig. 8, which is just the AOA for the idealized exponential tracer

² The dashed segments of the analytical solution curve are not computed but are instead interpolated linearly between the preceding and the following segments. This is done because expression (32) is not valid, even approximately, in the intervals between the times t_i , when the exponential growth rate changes and the times $t_i + z/w_e$, when the altitude z “feels” the effect of the new growth rate.



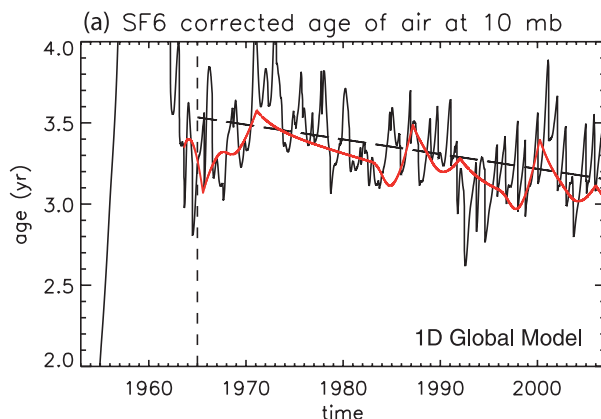
time-mean AOA: 3.247 years
AOA trend: -0.081 ± 0.001 years/decade

FIG. 8. AOA derived from the SF₆-like tracer using the numerical solution to the 1D global model (black) and the analytical solution (red) discussed in section 5. The dashed black line is a linear fit to the numerical solution for the SF₆-like tracer. The green curve is the AOA for an idealized tracer with constant linear growth rate. See text for details.

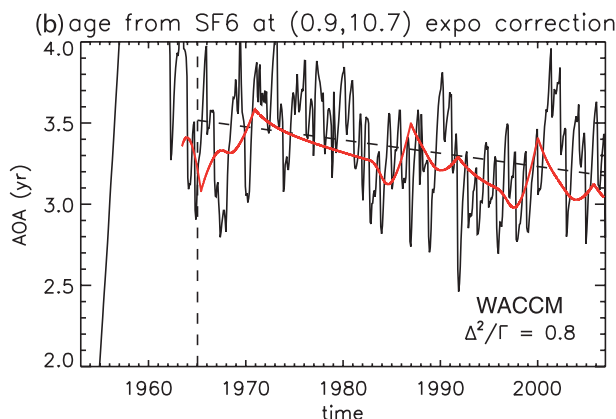
shown in Fig. 6b. The slope of the AOA curve for the SF₆-like tracer approximates that of the idealized exponential tracer only when the former experiences a relatively long interval of constant growth rate, between 1968 and 1983 (cf. Table 2). At other times the evolution of the SF₆-like tracer does not behave as expected for an exponentially growing tracer because a pure exponential profile is never established.

Figure 9 shows the AOA of the SF₆-like tracer superimposed on the AOA obtained when the actual SF₆ time series is used as the boundary condition in the 1D global model (top panel) and when SF₆ from WACCM is used to compute AOA (bottom panel). The AOA obtained from the SF₆-like tracer does a good job of following the long-term evolution of AOA derived from SF₆ itself, although there are differences in detail. These are not unexpected since the AOA for SF₆-like tracer is not influenced by interannual variations in transport. The AOA trend computed from the SF₆-like tracer is similar to that computed from SF₆ itself in both the 1D model and in WACCM. In all cases, these trends (about -0.08 to -0.09 yr decade⁻¹) are substantially smaller than the trend computed from a linear tracer, which is about -0.15 yr decade⁻¹. Taken together, Figs. 8 and 9 imply that AOA trends derived from SF₆ underestimate the trend in AOA implied by a linear tracer with a constant growth rate, even after applying the appropriate correction for the exponential growth of SF₆.

As regards CO₂, we have shown (Figs. 3a,c) that its AOA time series exhibits very large interannual variability, introduced by the seasonal cycle at the entry point into the stratosphere. In a numerical model with continuous



time-mean AOA: 3.344 years (3.207)
AOA trend: -0.091 ± 0.002 years/decade (-0.081)



time-mean AOA: 3.346 years (3.207)
AOA trend: -0.082 ± 0.013 years/decade (-0.081)

FIG. 9. Numerical solution for AOA derived from the SF₆-like tracer (red) superimposed on results obtained using SF₆ from (a) the 1D global model and (b) WACCM. Mean AOA and its trend derived from SF₆ are shown in red, in parentheses. AOA estimates are corrected for nonlinear growth as discussed in the text.

output this variability can be reduced by smoothing the time series at the base point before computing the AOA, as shown in Figs. 3b,d. The AOA computed after smoothing the CO₂ time series no longer contains large interannual variations, but this does not alter much the value of the AOA trend. This is surprising because the growth rate of CO₂ is quite slow, such that one would expect it to behave much as a linearly growing tracer.

To investigate further the behavior of AOA derived from CO₂, we proceed as for SF₆ and construct a “CO₂-like” boundary condition:

$$\text{CO}_2(t_i) = \text{CO}_2(t_{0i}) \exp(r_i t_i), \quad (38)$$

where t_i , r_i are defined in Table 3. Comparison of Tables 2 and 3 shows that the growth rate of CO₂ is, in general, at

TABLE 3. Specification of the time-dependent growth rate of the CO₂-like tracer.

Segment t_i (yr)	Growth rate (yr ⁻¹)
[1953, 1964]	0.0022
[1965, 1970]	0.0030
[1971, 1978]	0.0036
[1979, 1982]	0.0040
[1983, 2002]	0.0044
[2002, 2006]	0.0048

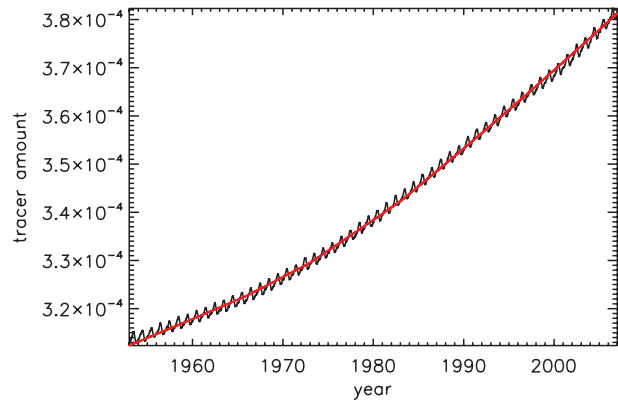
least a factor of 10 smaller than that of SF₆. Equation (38) does not include the strong seasonal cycle that CO₂ exhibits at the base point in the upper troposphere, but otherwise reproduces very well the long-term changes in CO₂, as shown in Fig. 10, where the series (38) is superimposed on the actual CO₂ time series at the base point.

Figure 11 shows the AOA calculated from the numerical solution³ of the 1D model using Eq. (38) as the lower boundary condition superimposed on the AOA obtained from CO₂ itself in the 1D model and in WACCM, after smoothing the CO₂ time series at the base point. The AOA derived from the CO₂-like tracer provides a good approximation to the long-term behavior of actual CO₂, yielding similar mean AOA and trend, especially compared to CO₂ in the 1D model. We note that mean CO₂ age from WACCM is systematically younger than the AOA in the 1D model. This difference may be due to the fact that CO₂ has a small source in the middle and upper stratosphere due to methane oxidation. This would tend to increase the CO₂ mixing ratio there and lead to a younger apparent mean age.

Consider, finally, the green curve superimposed on Fig. 11a, which shows the AOA for an idealized linearly growing tracer with uniform growth rate, as in Fig. 6a. Comparison of this curve with the AOA obtained from either the CO₂-like tracer or CO₂ itself shows that, as with SF₆, the AOA trend derived from CO₂ is affected by the adjustments that the AOA time series undergoes whenever there is a change in the growth rate of the tracer. Only during the long segment of uniform growth rate 1983–2002 does the trend in AOA derived from CO₂ approach that obtained from the idealized tracer with uniform linear growth rate. The longer-term trend (1965–2006) is substantially smaller.

6. Discussion and conclusions

We have used calculations of SF₆ and CO₂ for the period 1965–2006 made with the Whole Atmosphere Community

FIG. 10. As in Fig. 7, but for CO₂.

Climate Model to estimate stratospheric AOA and have shown that the trend in AOA derived from either of these tracers is substantially smaller than the trend inferred from an idealized, linearly growing tracer with uniform growth rate. This occurs even though a correction for nonlinear rate of growth has been applied to the AOA derived from SF₆ and CO₂; such a correction is important in the case of SF₆, which grows very rapidly with time, but turns out to be irrelevant for CO₂, whose growth rate is slow enough that the correction has negligible impact on the estimate of the AOA.

We have shown further that this result can be reproduced with a global 1D transport model of the global stratosphere formulated following Holton (1986) and that approximate analytical solutions to the simple global model can be obtained that shed light on this behavior. In particular, we showed that, in order to understand the evolution of AOA derived from natural tracers, one must consider the fact that their growth rates are not constant in time. The modification of AOA trends by changes in tracer growth rate is not predicted by the analytical solutions in section 5 for a tracer with an equilibrated global profile, or for that matter by the equivalent solutions for AOA derived earlier by Hall and Plumb (1994) using Green's function for the 1D global transport model described by Eq. (9). It is obtained here from the AOA derived from numerical solution of Eq. (9) and, approximately, from the analytical AOA solutions (20) and (32). In any case, it is evident that the nonuniform growth rates of SF₆ and CO₂ lead to underestimates of the AOA trend and make AOA trends derived from these natural species ambiguous proxies for trends in the stratospheric circulation. By contrast, a synthetic, linearly increasing tracer, such as used in WACCM and other models to estimate AOA, is perfectly well suited to the task, although attention must be paid to the fact that the magnitude of the fractional, or percentage, trend in AOA turns out to be

³ As was the case for SF₆, the analytical solution (not shown) agrees well with the numerical solution and supports the conclusion that changes in the evolution of the AOA are brought about by changes in the growth rate of CO₂.

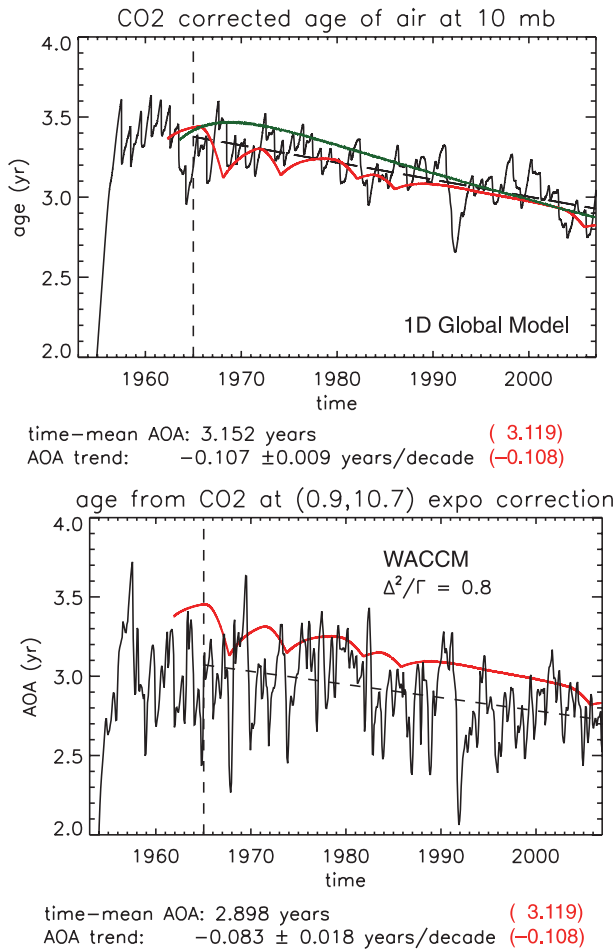


FIG. 11. As in Fig. 8, but for CO₂. The green curve in the top panel is the AOA for an idealized tracer with constant exponential growth rate. See text for details.

roughly twice as large as the trend in the mean meridional circulation, as shown in section 5a.

While the trends obtained here from SF₆ and CO₂ are small, they are negative and significantly different from zero, contrary to the results reported by Engel et al. (2009) based on observations of these tracers over the period 1975–2005. However, computation of the AOA from numerical model output has a major advantage over estimates based on data in that the former is available continuously everywhere in the model domain. The estimates of AOA discussed above are based on zonal-mean, monthly-mean results without any temporal gaps. The ability to work with zonal and monthly averages reduces greatly the “natural variability” present in the model. This, together with the temporal continuity and multi-decade length of the model output, yields AOA trends that are highly statistically significant. Thus, for example, AOA trends derived from WACCM output have a typical standard deviation of about ± 0.01 – 0.02 yr decade⁻¹,

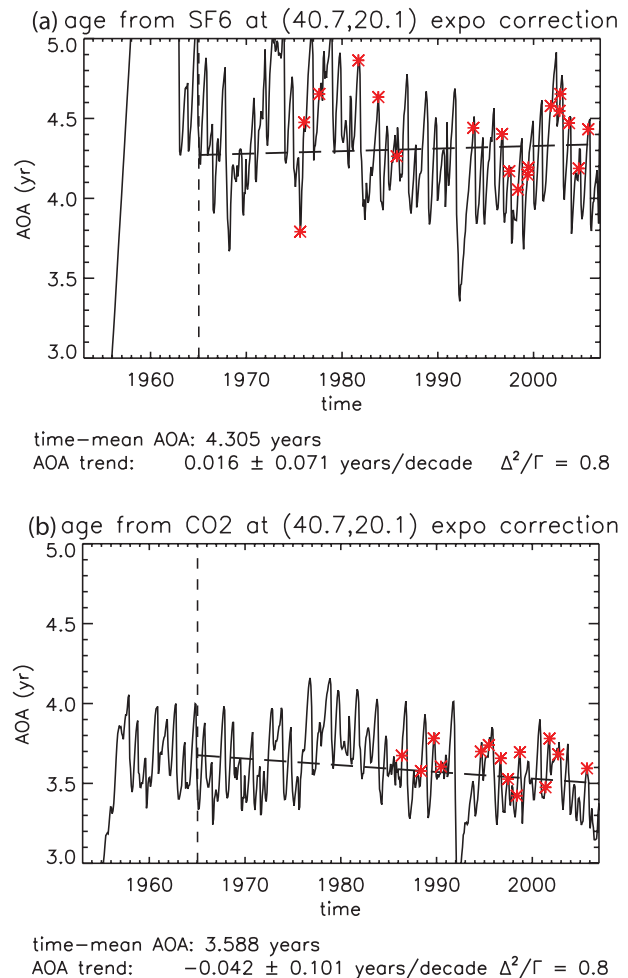


FIG. 12. AOA trends determined from WACCM (a) SF₆ and (b) CO₂ when the model is sampled using the same months and years as in the data analyzed by Engel et al. (2009), denoted by the red asterisks. The dashed lines are linear fits to the AOA of these restricted sets of data. See text for details.

whereas the standard deviation of the trends determined by Engel et al. from data are a factor of 10–20 larger. This is not surprising, since those trends are based on a sample size of 18 local observations for SF₆ and 14 for CO₂, obtained over a period of 30 yr.

What happens when WACCM results are sampled sparsely, as in the observations used by Engel et al. (2009)? Figure 12 shows midlatitude AOA trends obtained by sampling WACCM output for SF₆ and CO₂ on the same months and years as in the observations used by those authors. Two things are immediately apparent. First, the AOA trend derived from CO₂, while negative, is now very small and the trend derived from SF₆ is actually positive; second, the standard deviations become very large, about ± 0.1 yr decade⁻¹, which is roughly an order of magnitude larger than the standard deviations obtained

when the entire model output series are used. No particular significance should be attached to the actual values of the trends shown in Fig. 12 since slightly different (sparse) sampling can alter substantially their magnitude (and change their sign); but the fact that the standard deviation is now large compared to the trends underscores the point that trends determined from sparsely sampled data are highly uncertain.⁴ While the results of Fig. 12 are roughly consistent with those of Engel et al., there remains one puzzling difference in the case of CO₂. Our estimates of mean AOA for this tracer in the midlatitude stratosphere are about eight months younger than for SF₆, a result that may be due to the fact that we have not accounted for the effect of the stratospheric source of CO₂ from methane oxidation. However, in the results presented by Engel et al. the mean AOA is comparable for SF₆ and CO₂. We can offer no explanation at this time for the discrepancy, but it prevented our combining the AOA results for CO₂ and SF₆ to obtain an AOA trend based on both tracers, as was done by Engel et al.

Finally, it is important to bear in mind that in the case of SF₆, which has a very fast growth rate, application of a correction for nonlinear growth is essential for deriving AOA that can be compared to the AOA obtained from a linearly growing tracer. Here we have used a correction appropriate for exponential growth, as discussed in section 5 and in Hall and Plumb (1994). Our choice would appear to be justified by the ability to fit accurately the behavior of SF₆ by piecewise continuous exponential growth segments (see Fig. 7). However, other types of correction are possible, for example one that assumes that the growth rate can be approximated by a second-order polynomial. Such a quadratic fit and correction is discussed by Volk et al. (1997) and Waugh et al. (2003), and was used by Engel et al. (2009) in their analysis of SF₆ and CO₂. The effect of the correction method on the estimated mean age, let alone the trend, has not been investigated and must be considered another source of uncertainty in the determination of AOA trends from tracers with rapid growth rates.

In conclusion, the results presented here suggest that naturally occurring trace species are ambiguous proxies for trends in the circulation of the stratosphere. Waugh et al. (2003, section 5) arrived at similar conclusions in a study of tracer ages in the ocean. In principle, one could try to account for the biases introduced in the trend estimates by growth rates that vary in time but that would likely require uniform and continuous knowledge

of the evolution of the trace species, something that is readily available from a model but not from any existing observational dataset. It is possible, however, that evaluating the observations in the context of model results might provide a means for reducing the uncertainty in the estimate of the AOA trends.

Acknowledgments. The WACCM simulations were carried out at NCAR and at the NASA Advanced Supercomputing Division, Ames Research Center, CA. We thank Drs. A. Conley, J.-F. Lamarque, and A. K. Smith for their comments on the original version of the paper; and Dr. D. Waugh and an anonymous reviewer for their detailed and constructive reviews. We also thank Dr. A. Engel for very helpful discussions. Finally, we are grateful to Dr. D. Waugh for suggesting sources of information on the chemistry and tropospheric history of SF₆.

REFERENCES

- Austin, J., J. Wilson, F. Li, and H. Vömel, 2007: Evolution of water vapor concentrations and stratospheric age of air in coupled chemistry–climate model simulations. *J. Atmos. Sci.*, **64**, 905–921.
- Butchart, N., and Coauthors, 2006: Simulations of anthropogenic change in the strength of the Brewer–Dobson circulation. *Climate Dyn.*, **27**, 727–741.
- Engel, A., and Coauthors, 2009: Age of stratospheric air unchanged within uncertainties over the past 30 years. *Nat. Geosci.*, **2**, 28–31.
- Eyring, V., and Coauthors, 2006: Assessment of temperature, trace species, and ozone in chemistry–climate model simulations of the recent past. *J. Geophys. Res.*, **111**, D22308, doi:10.1029/2006JD007327.
- , and Coauthors, 2008: Overview of the new CCMVal reference and sensitivity simulations in support of upcoming ozone and climate assessments and the planned SPARC CCMVal. *SPARC Newsletter*, No. 30, SPARC Office, Toronto, ON, Canada, 20–26.
- Garcia, R. R., 1991: Parameterization of planetary wave breaking in the middle atmosphere. *J. Atmos. Sci.*, **48**, 1405–1419.
- , and W. Randel, 2008: Acceleration of the Brewer–Dobson circulation due to increases in greenhouse gases. *J. Atmos. Sci.*, **65**, 2731–2739.
- , D. R. Marsh, D. E. Kinnison, B. A. Boville, and F. Sassi, 2007: Simulation of secular trends in the middle atmosphere, 1950–2003. *J. Geophys. Res.*, **112**, D09301, doi:10.1029/2006JD007485.
- Hall, T., and R. Plumb, 1994: Age as a diagnostic of stratospheric transport. *J. Geophys. Res.*, **99**, 1059–1070.
- Holstlag, A. M., and B. A. Boville, 1993: Local versus nonlocal boundary layer diffusion in a global climate model. *J. Climate*, **6**, 1825–1842.
- Holton, J. R., 1986: A dynamically based transport parameterization for one-dimensional photochemical models of the stratosphere. *J. Geophys. Res.*, **91**, 2681–2686.
- Hurrell, J. W., J. J. Hack, A. S. Phillips, J. Caron, and J. Yin, 2006: The dynamical simulation of the Community Atmosphere Model, version 3 (CAM3). *J. Climate*, **19**, 2162–2183.
- Li, F., J. Austin, and J. Wilson, 2008: The strength of the Brewer–Dobson circulation in a changing climate: Coupled chemistry–climate model simulations. *J. Climate*, **21**, 40–57.

⁴ This is despite the fact that the sampling problem is ameliorated by the use of zonally and monthly averaged model output, which suppresses small-scale spatial variability and short-term temporal variability.

- Maiss, M., and C. A. M. Brenninkmeijer, 1998: Atmospheric SF₆, trends, sources, and prospects. *Environ. Sci. Technol.*, **32**, 3077–3086.
- Matthes, K., U. Langematz, L. L. Gray, K. Koder, and K. Labitzke, 2004: Improved 11-year solar signal in the Freie Universität Berlin Climate Middle Atmosphere Model (FUBC-MAM). *J. Geophys. Res.*, **109**, D06101, doi:10.1029/2003JD004012.
- McFarlane, N. A., 1987: The effect of orographically excited gravity wave drag on the general circulation of the lower stratosphere and troposphere. *J. Atmos. Sci.*, **44**, 1775–1800.
- McLandress, C., and T. Shepherd, 2009: Simulated anthropogenic changes in the Brewer–Dobson circulation, including its extension to high latitudes. *J. Climate*, **22**, 1516–1540.
- Pradayrol, C., A. M. Casanovas, I. Deharo, J. P. Guelfucci, and J. Casanovas, 1996: Absorption coefficients of SF₆, SF₄, SOF₂, and SO₂F₂ in the vacuum ultraviolet. *J. Phys. III*, **6**, 603–612.
- Richter, J. H., F. Sassi, and R. R. Garcia, 2010: Towards a physically based gravity wave source parameterization in a general circulation model. *J. Atmos. Sci.*, **67**, 136–156.
- Sander, S. P., and Coauthors, 2006: Chemical kinetics and photochemical data for use in atmospheric studies, evaluation no. 15. Jet Propulsion Laboratory Publ. 06–2.
- Tilmes, S., R. R. Garcia, D. E. Kinnison, A. Gettelman, and P. J. Rasch, 2009: Impact of geoengineered aerosols on the troposphere and stratosphere. *J. Geophys. Res.*, **114**, D12305, doi:10.1029/2008JD011420.
- Volk, C. M., and Coauthors, 1997: Evaluation of source gas lifetimes from stratospheric observations. *J. Geophys. Res.*, **102**, 25 543–25 564.
- Waugh, D. W., and T. Hall, 2002: Age of stratospheric air: Theory, observations and models. *Rev. Geophys.*, **40**, 1010, doi:10.1029/2000RG000101.
- , —, and T. Haine, 2003: Relationships among tracer ages. *J. Geophys. Res.*, **108**, 3138, doi:10.1029/2002JC001325.